2019 LANL contribution to Salt-GDSA Integration

Fuel Cycle Research & Development

Prepared for
US Department of Energy
Spent Fuel and Waste Science and Technology
Milestone M3SF-19LA010303012

P.H. Stauffer
J. J. Beisman
C.W. Gable
D.R. Harp
T.A. Miller
E.J. Guiltinan

Los Alamos National Laboratory
April 30, 2019

M. Ebeida
Sandia National Laboratory

Los Alamos National Laboratory Document
LA-UR-23322

FCT Quality Assurance Program Document

Appendix E
FCT Document Cover Sheet

Name/Title of Deliverable/Milestone	2019 LANL contribution to Salt-GDSA Integration
Work Package Title and Number	**SF-19LA010303012 Salt R&D - LANL**
Work Package WBS Number	1.08.01.03.03 - Salt Disposal R&D
Responsible Work Package Manager	Philip H. Stauffer
	(Name/Signature)
Date Submitted	

Quality Rigor Level for Deliverable/Milestone	☒ QRL-3	☐ QRL-2	☐ QRL-1 ☐ Nuclear Data	☐ N/A*

This deliverable was prepared in accordance with Los Alamos National Laboratory
(Participant/National Laboratory Name)

QA program which meets the requirements of
☒ DOE Order 414.1 ☐ NQA-1-2000

This Deliverable was subjected to:

☐ Technical Review
Technical Review (TR)
Review Documentation Provided
☐ Signed TR Report or,
☐ Signed TR Concurrence Sheet or,
☒ Signature of TR Reviewer(s) below
Name and Signature of Reviewers
Hari Viswanathan

☐ Peer Review
Peer Review (PR)
Review Documentation Provided
☐ Signed PR Report or,
☐ Signed PR Concurrence Sheet or,
☐ Signature of PR Reviewer(s) below

*Note: In some cases there may be a milestone where an item is being fabricated, maintenance is being performed on a facility, or a document is being issued through a formal document control process where it specifically calls out a formal review of the document. In these cases, documentation (e.g., inspection report, maintenance request, work planning package documentation or the documented review of the issued document through the document control process) of the completion of the activity along with the Document Cover Sheet is sufficient to demonstrate achieving the milestone. QRL for such milestones may be also be marked N/A in the work package provided the work package clearly specifies the requirement to use the Document Cover Sheet and provide supporting documentation.

Table of Contents

List of Figures

List of Tables

ACRONYMS

CBFO	Carlsbad field office (DOE-EM WIPP office)
CRDS	cavity ring-down spectrometer
DAKOTA	Design Optimization, Parameter Estimation, Uncertainty Quantification, and Sensitivity Analysis
DOE	Department of Energy
DOE-EM	DOE Office of Environmental Management
DOE-NE	DOE Office of Nuclear Energy
FEHM	Finite Element Heat and Mass Transfer
FY	fiscal year (October-September)
GDSA	geologic disposal safety assessment
LANL	Los Alamos National Laboratory
LBNL	Lawrence Berkeley National Laboratory
PA	performance assessment
PFLOTRAN	parallel flow and transport (simulation code)
R&D	research and development
SFWST	Spent Fuel & Waste Science & Technology (DOE-NE program)
SNF	Spent nuclear fuel
SNL	Sandia National Laboratories
THMC	thermal-hydrological-mechanical-chemical (also THM & THC)
TOUGH	Transport of Unsaturated Groundwater and Heat (simulation code)
URL	underground research laboratory
US	United States
WIPP	Waste Isolation Pilot Plant (DOE-EM site)

1. Introduction

The Spent Fuel and Waste Science and Technology (SFWST) Campaign of the U.S. Department of Energy (DOE) Office of Nuclear Energy (NE) is tasked with conducting research and development (R&D) related to the geological disposal of spent nuclear fuel (SNF) and high level nuclear waste (HLW). Two high priority topics for SFWST R&D are to create design concepts and numerical modeling approaches for disposal systems (DOE 2011). A major piece of the R&D work will be a Geologic Disposal Safety Analysis (GDSA) reference case for each of the studied rock types (salt, crystalline, argillite) (Mariner et al., 2018). The GDSA analysis is a form of typical Performance Assessment (PA) that relies on complex numerical simulations supported by experimental data to predict long-term radionuclide transport behavior (Mariner et al., 2018). Currently, PFLOTRAN, a reactive multi-phase flow and transport simulator (PFLOTRAN, 2019) and Dakota (Dakota, 2019), a stochastic uncertainty quantification tool, are being used as the primary drivers for GDSA calculations of long-term impacts as part of an overall GSDA Framwork (Figure 1-1). The current philosophy in GDSA design is to have less reliance on assumptions, simplifications, and model abstractions and include significant coupled (multiphysics) processes in three-dimensions (Seougian 2018).

One goal of the Geologic Disposal Safety Analysis (GDSA) is to integrate the results from a number of process-level simulation tools within the GSDA Framework. Examples of specific process-level simulation tools that are supporting the GDSA effort include VORCRUST (Vorocrust, 2019) developed by Sandia National Laboratory (SNL), TOUGH/FLAC (Blanco-Martin et al., 2018) developed by Lawrence Berkley National Laboratory (LBNL), and DFNWorks (dfnworks, 2019), LaGrit (LaGrit, 2019), and FEHM (FEHM, 2019) developed by LANL. A concerted effort is underway to understand how these supporting process-level simulation tools can be integrated within the GSDA Framework. A workshop held in January 2019 (2019 SFWST (UFD) R&D Roadmap Update Workshop) brought together researchers from the SFWST campaign to discuss progress on model integration and map out a path to address remaining issues over the next five years. Each of the primary repository rock types were given breakout groups to address their specific issues. Repository groups were also brought together in cross-cutting sessions. The workshop led to modifications of the SFWST goals and priorities and refocused efforts on integrating all aspects of the program within the GSDA Framework.

As part of the Spent Fuel and Waste Disposition (SFWD) program within the SFWST, LANL is supporting activities related to generic disposal in bedded salt formations. LANL's primary activities include design and implementation of field experiments (Stauffer et al., 2015; Johnson et al., 2017a; Boukhalfa et al., 2019; Figure 1-2), laboratory experiments, and numerical modeling (Jordan et al., 2015a+b; Bourret et al., 2016; Johnson et al., 2017b; Johnson et al., 2018; Bourret et al., 2019; Johnson et al., 2019).

As one task under LANL's Salt R&D work package, we participated in the 2019 SFWST (UFD) R&D Roadmap Update Workshop. Section 2 of this report summarizes our experience at the workshop and provides a review of the outcomes from the LANL perspective. Section 3 presents two examples of recent work by the Salt R&D group that could be included in the next iteration of the bedded salt GDSA reference case. Section 4 tackles numerical simulation integration issues and is broken into four subsections. Section 4.1 gives an example from our ongoing R&D of a code comparison exercise with suggestions for other code comparisons. In Section 4.2 we describe the impact of the Courant Number on the numerical dispersion of simulated contaminants. Dispersion is further discussed in Section 4.3. Section 4.4 presents a recently developed proposal to better integrate our numerical mesh generation capabilities.

This deliverable fulfills the Spent Fuel and Waste Disposition LANL Salt R&D Work Package Level 3 Milestone – 2019 LANL contribution to Salt-GDSA Integration (M3SF-19LA010303012)

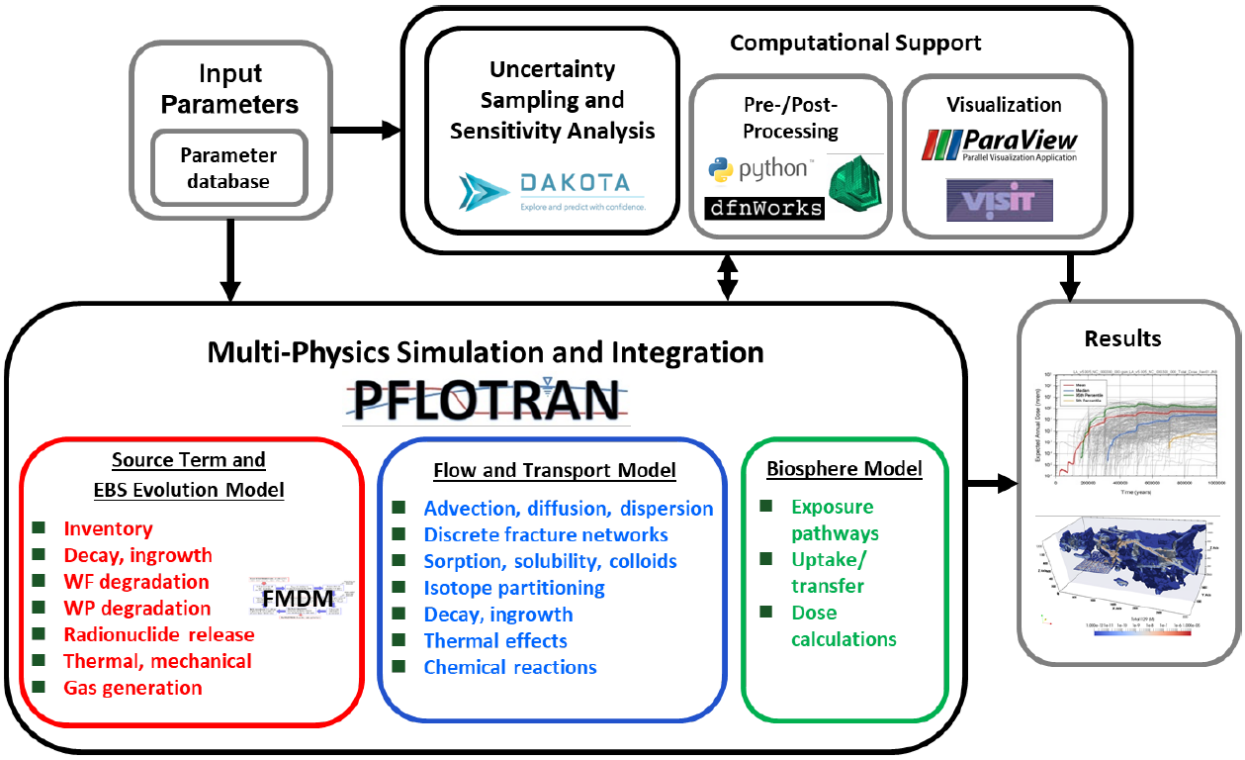

Figure 1-1 GDSA Conceptual Diagram (From Mariner et al., 2018)

Figure 1-2 Installation of an infrared heater in the WIPP underground.

2. Outcomes from the January 2019 SFWST Roadmap Update Workshop

In January 2019 LANL participated in the 2019 SFWST (UFD) R&D Roadmap Update Workshop. Specific to the Salt R&D work package, Dr. Stauffer and Dr. Guiltinan attended the salt breakout group. Dr. Stauffer also attended the cross-cutting breakout group to ensure that the salt GDSA revisions were represented. One goal of updating the R&D Roadmap is to ensure that GDSA integration is being addressed in the SFWST campaign.

2.1 Updates to generic Salt R&D priorities related to GDSA integration

Within the salt breakout group, the focus on the workshop was to revise the Salt R&D Activity Table spreadsheet to reflect progress during the last 8 years. Nearly all salt tasks were modified in some manner. State-of-the-Art Levels (SAL) were reduced for several of the tasks (S-2, S-6, S-9, and S-10; Table XX) based on the teams view that progress had been made in these areas. For example, S-9 was lowered from a SAL of 5 to a SAL of 3 because both FEHM and TOUGH/FLAC have well established models for dry-out; however coupled THC models in PFLOTRAN need to be further validated, with several salt dependent functions added for completeness. The recommendation from the workshop is to: “Perform code comparisons among PFLOTRAN, TOUGH, and FEHM on repository relevant simulations. Modeling will be calibrated on laboratory data and validated on field data”. S-10 was also lowered from a SAL of 5 to a SAL of 3 because drift renaturation can be handled in the process-level simulation tools; however this process is not currently in the GDSA salt repository reference case (SNL 2016).

In addition to reworking the SALs, the salt breakout group added three R&D tasks that the team agreed should be called out separately (S-11, S-12, and S-13). S-11 was added to acknowledge that little work has been done on the impacts of anhydrites, clays, and other non-salt components, especially in the presence of strong thermal gradients. These layers can be important because the permeability and porosity of bedded salt is such that non-salt layers may provide significant pathways or sources of brine, which can impact long-term performance. Further, non-salt layers have an impact on mechanical deformation. It was determined that we are not entirely sure of how to represent these layers in PA calculations, since they are small-scale heterogeneities. Integration of these layers into PA may require that a generic salt reference case include some effects of stylized non-salt layers. For the short-term, it was suggested that a process-modeling approach should be used to determine whether these features and their effects are important at repository time/length scales.

Table 2-1 Salt R&D Tasks. Tasks and values in green were modified.

R&D Task #	R&D Task (or Activity) Name	2019 SAL Numerical Value**	2019 ISC Numerical Value
S-1	Salt Coupled THM processes, hydraulic properties from mechanical behavior (geomechanical)	5	5
S-2	Salt Coupled THM processes, creep closure of excavations	4	5
S-3	Coupled THC advection and diffusion processes in Salt, multi-phase flow processes and material properties in Salt	5	5
S-4	Coupled THC processes in Salt, Dissolution and precipitation of salt near heat sources (heat pipes)	5	5
S-5	Borehole-based Field Testing in Salt	5	5
S-6	Laboratory Experiments to Validate Coupled Process models in Salt (in support of field test S-5)	3	5
S-7	Brine Origin, Chemistry, and Composition in Salt (in support of field test S-5)	4	5
S-8	Evolution of run-of-mine salt backfill	4	5
S-9	Numerical modeling of dry-out in multiphase	3	3
S-10	Drift re-saturation process in PA	3	3
S-11	THMC effects of anhydrites, clays, and other non-salt components	4	5
S-12	Laboratory testing and modeling of fluid inclusions	4	3
S-13	Acid gas generation, fate, and transport	5	3

Salt R&D task S-12 was included to highlight that more work is needed to understand the role of fluid inclusions in the short-term availability of brine. However it is assumed that fluid inclusions will be secondary to the long-term repository behavior, although it was suggested that a process-modeling approach is required to determine whether these features and their effects are important at repository time/length scales.

Salt R&D task 13 was added because of recent experimental results that showed significant hydrochloric acid formation from heating of WIPP salt above 150 °C (Stauffer et al., 2015). Acid gas generation may impact long-term performance in a secondary way, however it was acknowledged that a process-modeling and laboratory experimental approach is required to determine whether these features and their effects are important at repository time/length scales.

Figure 2-1 Oven Corrosion after Heating WIPP salt from Clay Seam F

3. Integration related to the Bedded Salt Repository Reference Case

In this section we discuss possible closer integration of salt process-level modeling with the current bedded salt reference case safety analysis. The most recent version of the bedded salt reference case is titled "Status of Progress Made toward Safety Analysis and Technical Site Evaluations for DOE Managed HLW and SNF" (Sevougian et al., 2016). In the Sevougian et al. (2016) analysis, the repository is designed using the in-drift concept where canisters are placed directly on the floor of the repository (Robinson et al., 2012). Additionally, the thermal load simulated for the bedded salt reference case is low because it is assumed to be a Defense Waste Repository (DWR).

The following two sections present integration issues that relate to recently developed experiments and simulations.

3.1 Permeability evolution of Run of Mine salt

Blanco-Martin et al. (2018) present simulations using TOUGH/FLAC that show the evolution of porosity and permeability in Run-of-Mine salt for up 100,000 years. We recommend that this work be used to help guide future choices for the timing of permeability changes in the GDSA

salt reference case. For example, in Figure 3-1, the permeability at 1000 y is estimated to be on order of 1 x 10^{-15} m^2. The current salt reference case backfill for a deterministic simulation is assigned a porosity of 0.113 and a permeability of 10^{-18} m^2 (Sevougian et al., 2016). For probabilistic simulations the salt reference case samples on porosity using a uniform uncertain distribution over the range 0.01 to 0.20. The differences in the simulated permeability as a function of porosity for salt backfill between the TOUGH/FLAC and PFLOTRAN models should be rectified as this parameterization could have significant impact on transport through the drifts, rooms, and halls during the first 1000+ years of the post-closure repository.

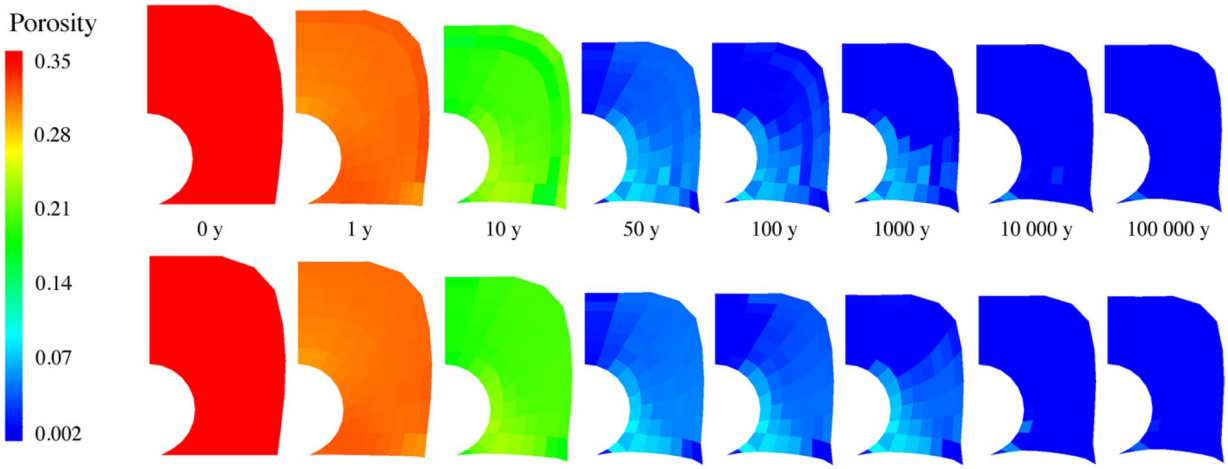

Figure 3-1 Porosity evolution for a generic salt repository: crushed salt porosity at different dates during the post-closure phase. Top: case including halite solubility constraints; bottom: case neglecting halite solubility constraints (Blanco-Martin et al., 2018)

3.2 Initial RoM Salt Porosity

Johnson et al. (2019) present simulations related to a canister that was buried under WIPP Run of Mine salt for nearly 9 months with 1000W of heating. Results from this analysis suggest that the initial porosity of the salt pile was close to 30%. The current salt reference case backfill is assumed to have an initial porosity of 35% (Sevougian et al., 2016). The newly estimated initial Run of Mine salt porosity can be used as input for both the TOUGH/FLAC and PFLOTRAN models. The new value is based on the thermal response of a large in-situ pile and is likely more robust than measurements taken on smaller samples.

Figure 3-2 Canister buried under a pile of WIPP Run of Mine salt.

4. Numerical Simulation Integration Issues

During work on a joint SNL/LANL alluvial basin modeling task for the SFWD project, it has become apparent that the underlying simulation tools being used in the GSDA and supporting process-level modeling tasks need to be better understood in relationship to the various flow and transport details. This section points out some of the issues that our team has found when trying to integrate FEHM simulations with PFLOTRAN. Implications for the GSDA are broad, including needing a set of guidelines on how to ensure that numerical problems do not dominate output.

The section is divided into distinct parts. First, we describe a modeling integration task done to confirm that the FEHM process level simulator and PFLOTAN, the GDSA simulation tool, generate the same output for an example test problem. Next, in Section 3.2 we describe the impact of the Courant Number on the numerical dispersion of simulated contaminants. Dispersion is further discussed in Section 3.3. Section 3.4 presents a recently developed proposal to better integrate our numerical mesh generation capabilities. Finally, in Section 3.5 we present a code comparison table that can form the basis for migrating capabilities from FEHM to PFLOTRAN.

4.1 Comparison of FEHM and PFLOTRAN simulation

Model integration includes ensuring that basic physical processes behave the same in the different process-level simulation tools used by the SFWD program. An example of this is included to demonstrate ongoing efforts to integrate physical processes into PFLOTRAN and verify their behavior. This example ties directly to the 2019 SFWST R&D Activities Table under

Salt R&D Task S-9 (Numerical modeling of dry-out in multiphase). The following example is modified from Bourret et al. (2016).

We constructed a simple test problem to confirm that the newly-modified macro *ngas* for FEHM (Jordan et al., 2015a) is accurately simulating flowing air with prescribed relative humidity. Comparison with analytical solutions confirm the code modifications are performing correctly. The goal is to specify relative humidity and temperature boundary conditions for flowing air to test that FEHM will transport water in vapor form in and out of a salt deposit as expected. The test problems examines dry air flow through a domain at a constant temperature. The dry air removes water from the porous salt matrix. This test problems show that the FEHM *ngas* successfully dries or saturates the salt matrix depending on temperature and relative humidity conditions. The validated example is then run with PFLTORAN as part of GDSA model integration.

Test 1: Constant temperature with a specified air relative humidity for in-flow

The grid for all *ngas* macro tests is a 1.0 m long, 0.2 m wide 2-dimensional space (Figure 1). It is discretized into 20 square, equally-sized elements. Material properties are initially homogeneous throughout the interior of the grid. Top (y = 0.2 m) and bottom (y = 0 m) boundaries are no-slip and no-flow. Air at specified temperature and humidity flows into the model along the line of nodes at x = 0, and flow out at x = 1.0. Nodes are initially partly saturated and will become either drier or wetter as relative humidity of flowing air changes.

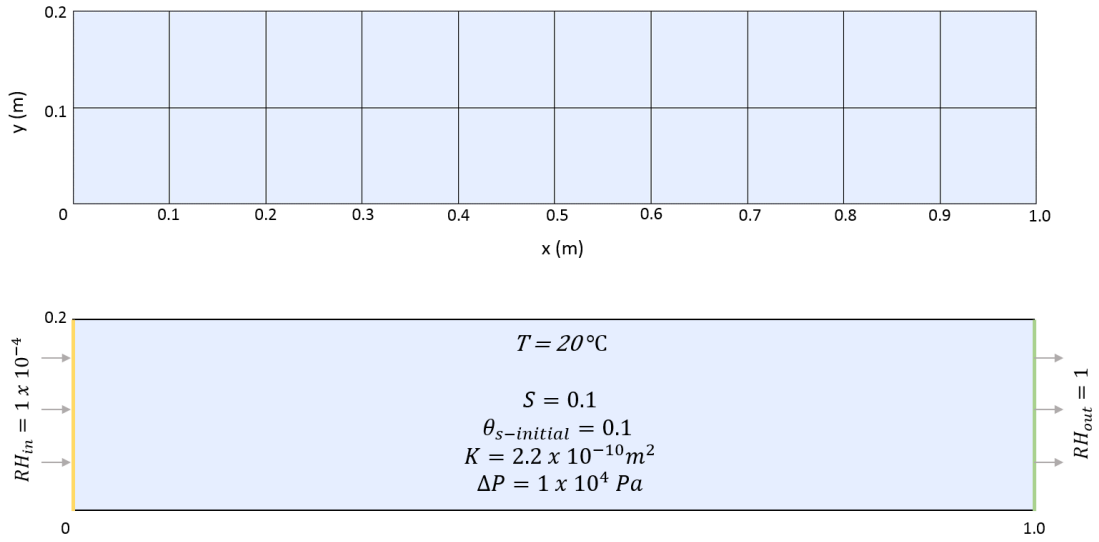

Figure 4-1: Model domain conceptualization, where RH is the relative humidity (-), n is the porosity (-), $\theta_{s-initial}$ is the initial saturation (-), K is the rock permeability (m^2), and ΔP is the pressure change between the right and left boundaries (Pa).

The domain has a constant temperature of 20 ºC and a very low, constant pressure gradient to drive air flow of $1\ x\ 10^{-4}\frac{pa}{m}$. The matrix is homogenous and isothermal, assigned values 0.1 for porosity and $2.2\ x\ 10^{-10}\ m^2$ for rock permeability. The initial saturation of the matrix is 0.1, results in 2 kg of initial water mass in the system. The mass of the pore-water represents the liquid water that the dry air ($RH = 1\ x\ 10^{-4}$) flowing through the domain can pick up and remove from the system in the vapor phase. We assigned a relative permeability of water to a value of zero, causing the water in the matrix to only be removed by transition into the vapor phase and not flow due to the pressure gradient. The air leaving the model has a relative humidity of 1.0.

The dry air enters the box at 20° holding $1.0\frac{g}{kg}$ of water, but has the capacity to hold $14.62\frac{g}{kg}$ which causes the air to pick up water from the matrix as it flows through the domain. The values of air moisture-holding capacity are determined by Equation 1 and shown in Figure 2, which was based on data available from engineering toolbox (http://www.engineeringtoolbox.com/humidity-ratio-air-d_686.html):

$$\phi_s = (4.4297x10^{-3})e^{0.0594T} \qquad \textit{Equation 1}$$

where T is temperature (℃) and ϕ_s is the air moisture-holding capacity $\left(\frac{kg}{kg}\right)$.

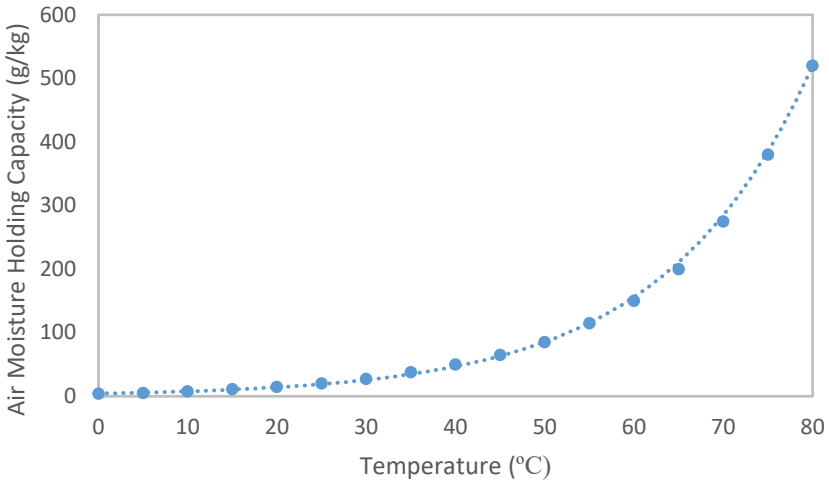

Figure 4-2: Maximum relative humidity curve shows the water vapor holding capacity of air at increasing temperatures.

An analytical solution was used to compare and test the correctness of the FEHM solution. The rate of water removal from the analytical solution was determined by Equation 2,

$$q_{water} = q_{air} * HR_{max} \qquad \textit{Equation 2}$$

where q_{water} and q_{air} is the mass flux of water and air $\left(\frac{kg}{s}\right)$, and HR_{max} is the moisture holding capacity of air $\left(\frac{kg}{kg}\right)$. The moisture holding capacity increases with temperature, so for this problem we expect air to pick up water as the temperature increases through the domain. The maximum air-moisture holding capacity is determined from the curve described by Equation 1.

Initial water mass, air-flow rate, temperature, and mass fraction water vapor of inflowing air were assigned the same values for the analytical solution and FEHM model. The comparison of the water-mass removal results, shown in Figure 3, are in agreement. As expected, the dry air evaporates the pore-water as it travels through the domain, thus drying out the matrix over time. The rate of water removal in the FEHM simulation matches with our simple analytical model, signifying FEHM is performing well. We also worked with Glen Hammond of Sandia National Laboratory to run the same numerical problem with PFLOTRAN, showing results that are nearly identical to FEHM and the analytical solution.

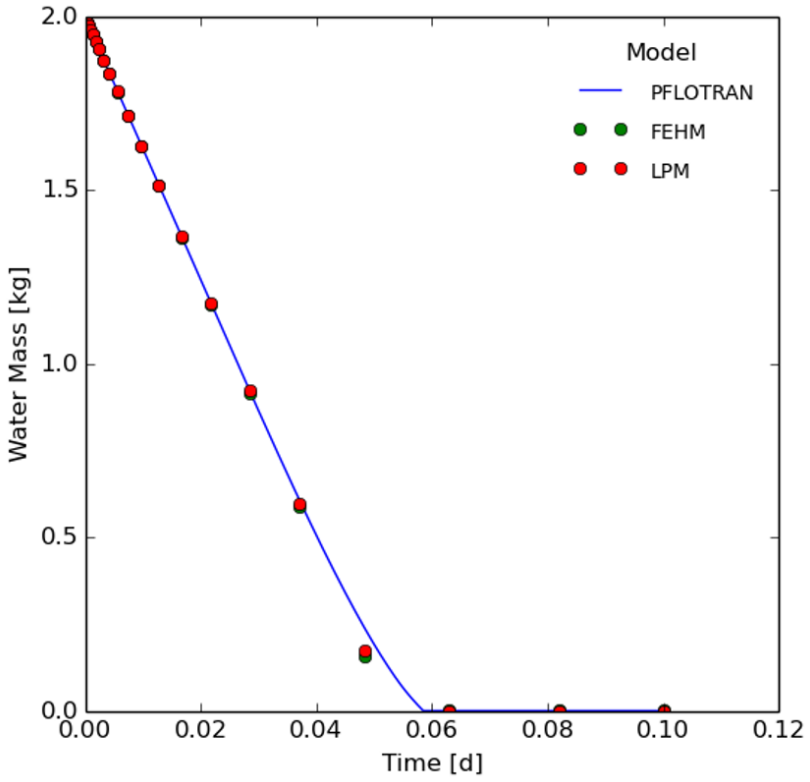

Figure 4-3: Comparison of FEMH and PFLOTRAN to the analytical solution for test problem 1.

4.2 Impact of Courant Number on numerical dispersion

Issues with numerical dispersion in PFLOTRAN have been previously addressed by Harp et al., 2018. Here we reprint Appendix A.2 from this work. We suggest that a path forward on model integration should include detailed analysis of when numerical dispersion is likely to impact GDSA calculations. Equation and figure numbering in this extracted appendix are left intact.

++++++++++++++++++ THE FOLLOWING is from HARP at al. (2018) ++++++++++++

Assuming uniform Darcy (volumetric) flux in the horizontal direction q_x, zero source or sink Q_c, tortuosity τ of 1, uniform air-filled porosity ϕ_a, and zero molecular diffusion and dispersion ($D^* = 0$), Eqs. 1 and 4 simplify to

$$\phi_a \frac{\partial \rho_a}{\partial t} = -\frac{\partial q_x \rho_a}{\partial x} \tag{15}$$

and

$$\phi_a \frac{\partial C_g}{\partial t} = -\frac{\partial^2 q_x C_g}{\partial x^2}, \tag{16}$$

respectively. If we consider an initial release of gas within the first upstream 10 m of the model, as described by initial and boundary conditions of

$$\begin{aligned} \text{i.c.:} & C_g = C_{g,0} \text{ at } t = 0,\ 0 < x < 10, \\ \text{b.c. 1:} & C_g = 0 \text{ at } t > 0,\ x = 0, \\ \text{b.c. 2:} & C_g = 0 \text{ at } t > 0,\ x = 100, \end{aligned} \tag{17}$$

the following solution describes purely advective flow:

$$C_g(x,t) = \begin{cases} C_{g,0}, & \text{if } 0 \le x - u * t \le 10 \\ 0, & \text{otherwise.} \end{cases} \tag{18}$$

Numerical solutions of the ADE (Eq. 4) are known to suffer from numerical dispersion. While previous investigations have focused on numerical dispersion in aqueous systems, an analysis involving gas transport is important here given the faster flow rates of gases in fractured rock. The Courant number,

$$Co = \frac{\Delta t q_x}{\Delta x}, \tag{19}$$

is a commonly used metric to determine if numerical dispersion will be significant for a given time step size Δt, velocity q_x, and mesh spacing Δx. While previous investigations have focused on numerical dispersion in aqueous systems, the following analysis is important given the faster flow rates of gases in fractured rock.

We evaluate the use of the Courant number for estimating numerical dispersion for our approach by estimating the apparent macrodispersivity of PFLOTRAN simulations with various Courant numbers. We ran PFLOTRAN simulations based on Eqs. 15 and 16 and initial and boundary conditions defined in equation 17 for all permutations of the following factors: (1) 1, 5, and 10 mm mesh spacing; (2) 1,10, and 100 h time step, and (3) 0.01, 0.1, and 1 $m^3/d/m^2$ uniform volumetric flux q_x (note that these are equal to pore velocities (m/s) in this case because $\phi_a = 1$), corresponding to Courant numbers ranging from $\sim$ 0.042 to $\sim$ 4200.

Macrodispersivity can be estimated based on the spatial extent of the plume (Dagan 1990) as

$$a = \frac{1}{2q_x}\frac{\partial(\sigma_x^2)}{\partial t}, \tag{20}$$

where σ_x^2 is the spatial variance of the plume, which is calculated based on spatial moments of the gas plume as

$$\sigma_x^2(t) = \frac{1}{C_T}\int x^2 C(x,t)dx - \mu_x^2(t), \tag{21}$$

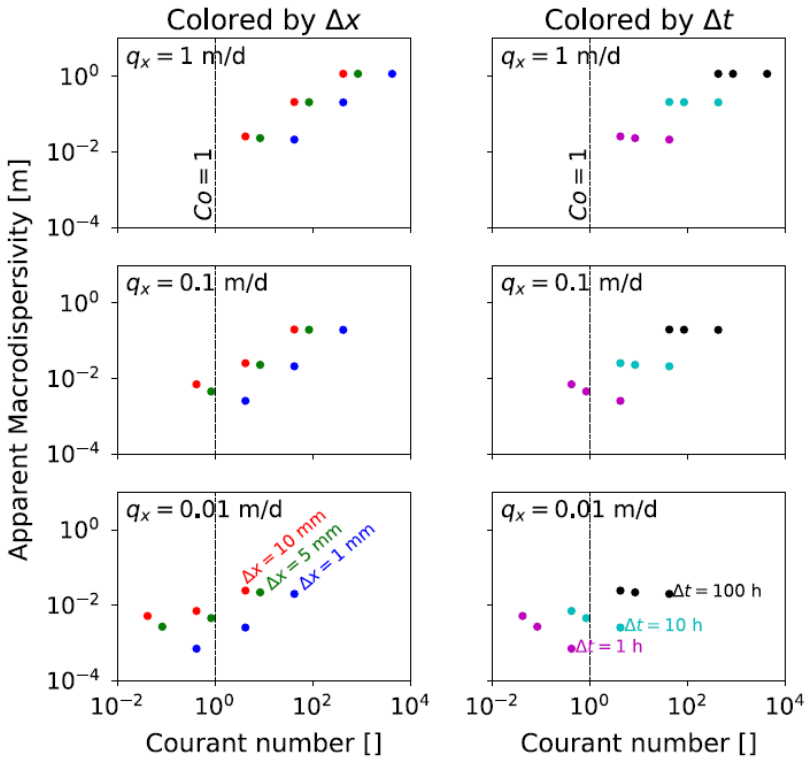

Fig. 11 Apparent macrodispersivity due to numerical dispersion as a function of Courant number for combinations of velocity q_x, mesh discretization Δx, and time step size Δt

where $C_T = \int C(x)dx$ and μ_x is the spatial mean of the plume calculated as

$$\mu_x(t) = \frac{1}{C_T}\int xC(x,t)\mathrm{d}x. \tag{22}$$

In order to estimate the variance due to numerical dispersion $\sigma^2_{x,n}$, the variance of purely advective flow, estimated by the uniform distribution, $\sigma^2_{x,a}(t) = \frac{(x_{max}(t)-x_{min}(t))^2}{12}$ is subtracted from σ^2_x

$$\sigma^2_{x,n}(t) = \sigma^2_x(t) - \sigma^2_{x,a}(t). \tag{23}$$

Substituting Eq. 23 into 20 for σ^2_x gives the apparent macrodispersivity due to numerical dispersion as

$$a_n = \frac{1}{2q_x}\frac{\partial(\sigma^2_{x,n})}{\partial t}. \tag{24}$$

Figure 11 contains plots of the apparent dispersivity due to numerical dispersion as a function of Courant number. The circles in the left and right columns of plots are colored by Δx and Δt, respectively, and q_x decreases down the rows of plots. The general rule that smaller Co results in less numerical dispersion is supported by Fig. 11 as Co and a_n both increase with increasing Δt and q_x; however, increasing Δx increases a_n, contrary to the rule defined by the Courant number (Eq. 19). Therefore, the contrary effect of Δx when using the Courant number as an indicator of numerical dispersion must be considered.

Figure 12 contains plots of relative concentration transects for the models with large and small numerical dispersion for $q_x = 0.01,\ 0.1,\ 1\ \mathrm{m^3/d/m^2}$. The purely advective transport of gas has reached the same location ($\sim$ 46.5 m) for each uniform velocity q_x, but at different times. Based on these plots, it is possible to approach the analytical solution, but this requires small Δx and Δt. Mitigation of numerical dispersion for meter per day flow rates, while possible through increased spatial and temporal discretization, may be computationally

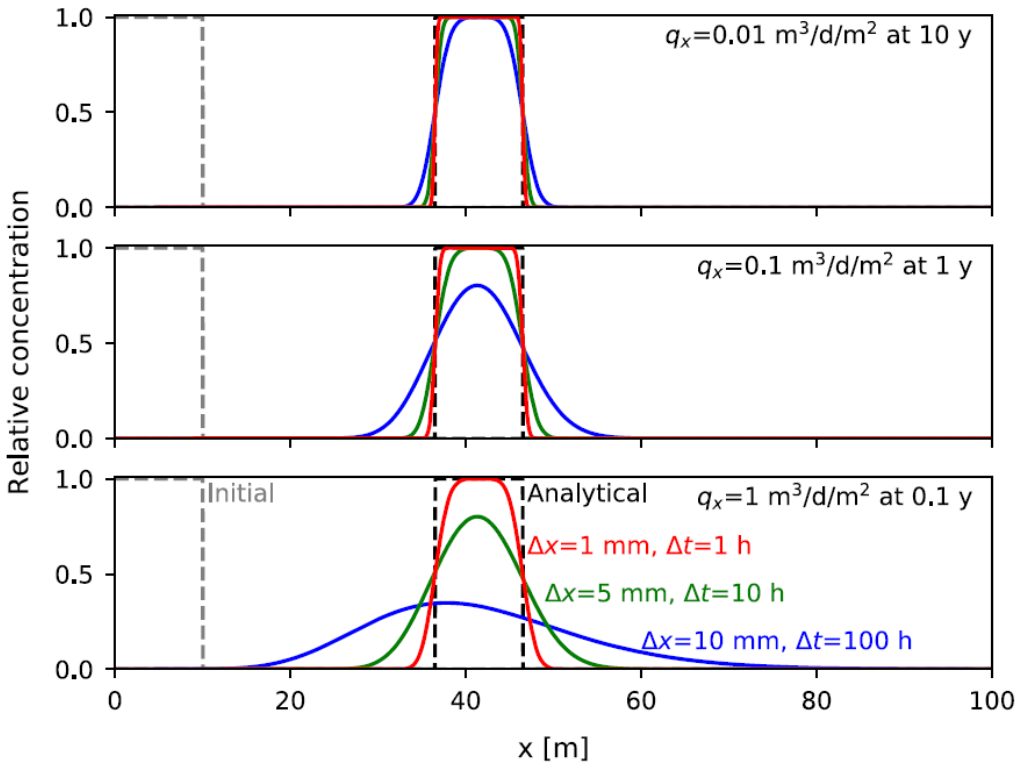

Fig. 12 Comparison of numerical approach to analytical solution of purely advective gas transport. The rows of plots present results for uniform flow rates of $u = 0.01$, 0.1, and 1 m/d and times of 10, 1, and 0.1 years, respectively. The initial concentration for all models is shown as a dashed gray line, and the analytical solution in each scenario is shown as a black dashed line. The colored lines in each plot are for combinations of spatial discretization Δx and time step size Δt labeled in the bottom plot

challenging for large models. Implementation of higher order solutions of Eq. 4 (Lax and Wendroff 1960; Liu et al. 1994) or particle tracking approaches (Painter et al. 2012) could be used to reduce the numerical dispersion and should be explored further for modeling gas transport in fractured rock.

++++++++++++++++++ This marks the end of Appendix A2 of Harp et al., 2018. ++++++

4.3 Numerical dispersion effects in reactive flows

The fate and transport of subsurface contaminants are often dominated by advection, where solutes flow with the bulk fluid phase. Unfortunately, as shown in Section 5.1, spurious dispersion in the numerical solution of the advection equation is a serious issue. This numerical dispersion results in the smearing of spatial concentration gradients, causing solutes to artificially spread and decreasing time to breakthrough. Numerical dispersion can significantly affect the simulation of reactive flows. In these simulations, reactions occur when chemically distinct solutes converge or a solute follows a flowpath through a reactive substrate. Numerical dispersion artificially enhances solute mixing, which increases the amount and spatial extent of reaction products. Numerical dispersion conveniently mimics hydrodynamic dispersion, but the

magnitude of numerical dispersion is dependent not upon any physical property, but on the level of grid refinement, which makes calibrating the process very challenging.

Accurate numerical approximation of linear scalar advection is difficult. Despite many advancements in the modeling of fluid flow in porous media, no universally-accepted, accurate and efficient algorithm has been developed to solve it. Any method for solving the linear scalar advection equation will produce some level of numerical dispersion. Fortunately, higher-order approximations of the advection term can significantly decrease the false solute spreading caused by numerical dispersion. The remainder of this section will be used to demonstrate the difference in performance between a first-order and higher-order advection scheme. The first-order scheme is the standard donor-cell upwind method, and is first-order accurate in time and space. The higher-order scheme is a variant of the Lax-Wendroff scheme, and is second-order accurate in time and space. Both schemes are integrated in time with the forward Euler method.

4.3.1 Grid Convergence Test

To evaluate the basic performance and relative accuracy of these schemes, we have simulated, with varying degrees of grid refinement, a one-dimensional square tracer profile traveling at a constant velocity. While this is a simple test case, the discontinuities in solute concentrations at the leading and trailing edge of the tracer profile are numerically challenging to resolve, and provide a reasonable approximation of the relative magnitude of numerical dispersion produced by each scheme. We use eight different levels of grid refinement to represent a 100 m long domain, ranging from 20 to 2560 nodes (20, 40, 80, 160, 320, 640, 1280, and 2560 nodes). The CFL number used in these simulations is 0.3 and the tracer profile is transported 50 m, requiring *ceiling* $(\frac{n}{2CFL})$ iterations, where n is the number of nodes. Figure 4-4 shows the results of the simulations. The higher-order scheme produces a closer approximation of the analytical solution with 80 nodes than does the first-order scheme at the finest level of grid refinement, 2560 nodes. Table 4-1 shows the error norms for the 320-node simulation. The higher-order scheme suffers from less error in all norms.

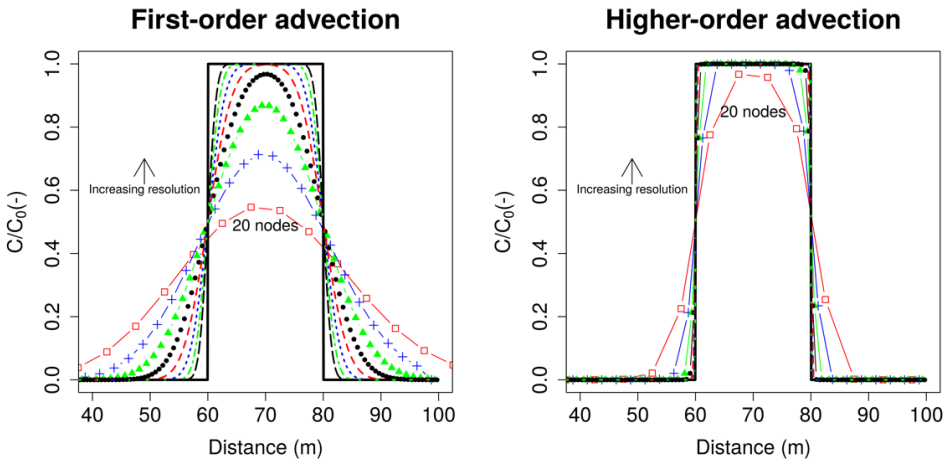

Figure 4-4 Results from the grid convergence test. The solid black line is the analytical solution. The lines with symbols are the simulation results. The levels of grid refinement, from coarsest (most dispersive) to finest (least dispersive), are 20, 40, 80, 320, 640, 1280, and 2560 nodes

Table 4-1 Error norms of Transport Schemes in 320-node simulation

Scheme	L_1 error	L_2 error	L_{inf} error
First-order	16.88	2.223	0.4837
Higher-order	0.9423	0.4492	0.2345

4.3.2 Reactive Transport Comparison

In order to evaluate the influence different advection schemes can have on mixing-induced reactions, we simulate reactive flow in a three-dimensional domain (Figure 4-5) with a spatially-variable velocity field. Two generic reactions are considered, instantaneous and reversible aqueous speciation,

$$A + B \longleftrightarrow C_{aqueous}, \quad k = 10^{0.777},$$

and the kinetic formation of a solid mineral from aqueous components,

$$A + B \rightarrow C_{mineral}, \quad k = 10^{-8.3}, R = 10^{-8.5}\ (mol\ m^{-2}\ s^{-1}).$$

The grid for these simulations is 160 x 40 x 40 nodes, representing a 10 x 2.5 x 2.5 m domain. A Dirichlet-style constant head condition is imposed on the x-direction domain boundaries and a no-flow condition is imposed on all other domain boundaries. A hydraulic gradient of 0.1 (-) in the positive X direction drives saturated flow through a domain with a spatially variable hydraulic conductivity field (Figure 4-5). As solution A mixes with solution B, the two reactions shown above proceed.

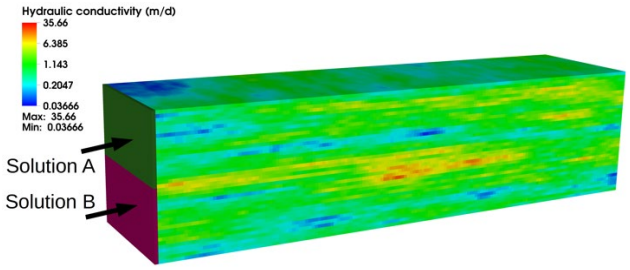

Figure 4-5 Problem setup and hydraulic conductivity field used in the reactive transport simulations.

Results of the reactive transport comparison show that the first-order scheme produces more reaction product than the higher-order scheme (Figure 4-6). At a time of 7 days, when the simulation ends, the effective mineral reaction rate produced by the first-order scheme is 47.2% faster than that of the higher-order scheme, and the mass of aqueous reaction product is 74.8% larger. Visual inspection and comparison of aqueous reaction product plumes at 7 days (Figure 4-7) shows the magnitude of the spatial spreading caused by numerical dispersion.

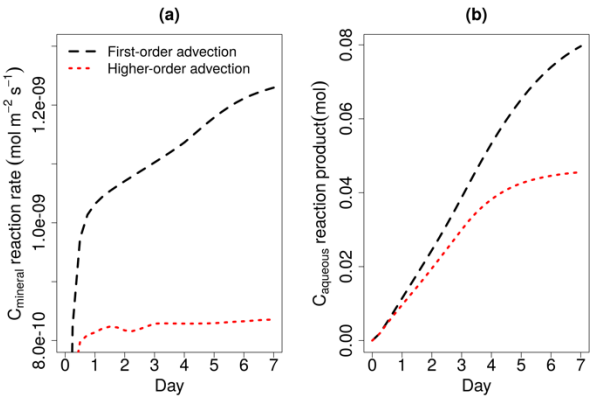

Figure 4-6 Effective mineral reaction rate (a) and moles of aqueous reaction product (b) produced by each scheme

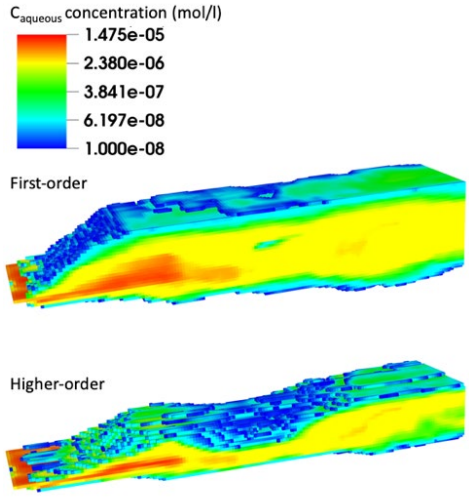

Figure 4-7 Aqueous reaction product plumes produced by the different schemes at a simulation time of 7.0 days.

4.3.3 Concluding Remarks

The numerical dispersion inherent in low-quality advection schemes can have a significant effect in simulations of reactive flow. First-order approximations of advective transport should be avoided in cases where time of breakthrough, preservation of sharp spatial concentration gradients, or the amount and spatial extent of mixing-induced reaction products is an important feature.

4.4 Numerical mesh integration issues

During work on a joint SNL/LANL alluvial basin modeling task for the SFWD project, it has become apparent that the underlying numerical meshes being used in the GSDA and supporting process-level modeling tasks need to be more well understood in relationship to the various flow and transport simulation packages (PFLOTRAN, FEHM, TOUGH). To tackle this issue, LANL and SNL have initiated a proposal that will be undertaken jointly through several funded work

packages that the numerical mesh issues impact (crystalline, argillite, salt, alluvial basin). The text of the proposal is included below. The vison of the proposal is summarized by the following quote

> *"We believe that if a streamlined workflow can be developed, this technology could lead to an entirely new, much less labor intensive, way to generate high quality meshes for geologic applications of flow and transport in porous media."*

Proposal for joint support by Los Alamos National Laboratory and Sandia National Laboratory by SFWD-SFWST program for evaluation and prototyping the use of VoroCrust software for computational model mesh generation and model setup with applications to underground repository flow and transport modeling.

Over the past year Ebeida (SNL), Gable (LANL), Miller (LANL) have been informally exchanging ideas and data and have made the first steps in exploring the use of VoroCrust for mesh generation and model setup for geologic applications. Based on these informal exchanges, we believe that collaboration and development of a workflow utilizing VoroCrust for mesh generation and model setup for geologic applications of flow and transport using the flow in porous media codes PFLOTRAN and FEHM offers great promise. This is a request for support from SFWD-SFWST program to provide financial support of a collaborative effort outlined below.

We believe that if a streamlined workflow can be developed, this technology could lead to an entirely new, much less labor intensive, way to generate high quality meshes for geologic applications of flow and transport in porous media.

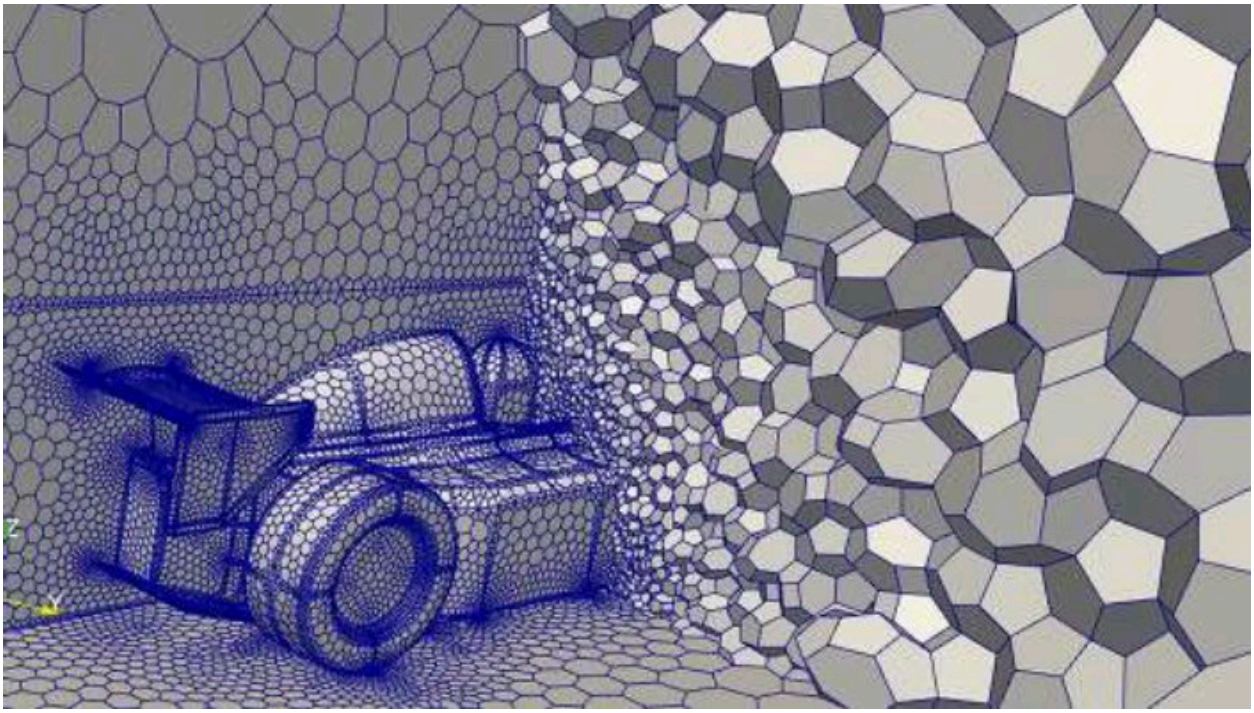

Figure 4-8 Example Vorocrust mesh.

1. **Motivation**
    a. Modeling of repository performance is an important tool for evaluation of potential underground repository performance
    b. Mesh generation is a tough problem in the modeling workflow
    c. Flow and transport applications have some particularly challenging characteristics
        i. Input geometry is seldom engineering CAD format
        ii. High aspect ratio geometry
        iii. Control Volume solvers that utilize two point flux approximation (PFLOTRAN, FEHM, TOUGH2) are most accurate when the mesh is Voronoi polyhedral control volume
    d. VoroCrust offers an automated approaches to solving some outstanding problems in mesh generation and model setup
2. **Current Approach**
    a. Geologic Framework Models (EarthVision, Jewel Suite)
    b. Mesh Generation for applications using Control Volume solvers
    c. Target physics, heat and mass transport in geologic porous media
    d. Target codes (PFLOTRAN, FEHM, TOUGH2/3)
    e. Drawbacks of current approach
        i. Very labor intensive when geometry is complex
        ii. Even with a lot of manual intervention, difficult to get it perfect
        iii. Current approach is using Delaunay meshing to derive dual Voronoi control volume instead of direct polyhedral meshing

3. **VoroCrust**
    a. The first algorithm to generate Conforming Voronoi meshes for non-convex domains with curved boundaries.
    b. A provably correct algorithm with bounds on numerous quality metrics of the generated Voronoi cells (e.g. aspect ratio, dihedral angles,…).
    c. The generated polyhedral cells are true Voronoi Cells that are not clipped and hence they maintain convexity, planarity of faces and orthogonality between faces and their dual Delaunay edges.
    d. Since the Output is an unclipped Voronoi Tessellation, it is uniquely defined by the locations of the Voronoi Seeds and hence an explicit element storage is not needed.
    e. VoroCrust is an award winning technique (Up & Coming Innovation award in 2018 from Sandia National Laboratories) and has 3 pending patents.
    f. A VoroCrust prototype has been release in August 2018. Our main goal here is to demonstrate it on full scale applications.
4. **Proposed Work**
    a. Scope:
        i. Test current VoroCrust capabilities on relevant geological model geometry:
            1. GDSA UZ Reference Case
            2. GDSA Shale Reference Case
            3. Heater test experiments at salt repository models modeling heat and moisture transport at WIPP underground test
            4. TBD, prototype contributions from SNL
            5. Test cases using existing complex geological framework models
        ii. Prototype workflow to prepare geologic framework models for input to VoroCrust
        iii. Prototype workflow to prepare VoroCrust output for input to PFLOTRAN and FEHM
        iv. Identify obstacles or areas that would require further development to create a production level mesh generation workflow
        v. Work with customers (SNL, LANL) to develop prototype workflows that take complex geologic model input and produce Voronoi control volume mesh that can be ingested into solvers (PFLOTRAN, FEHM) and provide necessary infrastructure for setting boundary conditions, material properties, and initial conditions
    b. Team
        i. Mohamed Ebeida, Discrete Math and Optimization, Sandia National Laboratories

   ii. Carl Gable, Computational Earth Science, Los Alamos National Laboratory
   iii. Terry Miller, Computational Earth Science, Los Alamos National Laboratory
   iv. Daniel Livingston, Computational Earth Science, Los Alamos National Laboratory
c. Customers
   i. Hari Viswanathan, LANL
   ii. Phil Stauffer, LANL
   iii. Emily Stein, SNL
   iv. Glenn Hammond, SNL
d. Schedule
   i. All scoping and prototype work to be completed in FY19

5. References

Beauheim, R. L., P. S. Domski, and R. M. Roberts (1999), *Hydraulic Testing of Salado Formation Evaporites at the Waste Isolation Pilot Plant Site: Final Report*, Sandia National Laboratory, Report: SAND--98-2537

Blanco-Martín, L., J. Rutqvist, A. Battistelli, J.T. Birkholzer, (2018), *Coupled processes modeling in rock salt and crushed salt including halite solubility constraints: Application to disposal of heat-generating nuclear waste*, Transport in Porous Media 124, 159-182

Boukhalfa, H., S. Ware, P.J. Johnson, S. Otto, D. Weaver, B. Dozier, M.M. Mills, C. Herrick, K.L. Kuhlman, P.H. Stauffer, (2019), *Development of an Experimental Approach for Thermal Testing in Bedded Salt*, Waste Management 2019 Proceedings

Bourret, S. M., E. J. Guiltinan, P. J. Johnson, S. Otto, D. J. Weaver, B. Dozier, H. Boukhalfa, T. A. Miller, and P. H. Stauffer (2019), *Experiments and Simulation of a Borehole in Salt to Understand Heat, Brine, and Vapor Migration*. Waste Management 2019 Proceedings

Bourret, S.M., P.J. Johnson, G.A. Zyvoloski, S.P. Chu, D.J. Weaver, S. Otto, H. Boukhalfa, F.A. Caporuscio, A.B. Jordan, P.H. Stauffer, (2016), *Experiments and Modeling in Support of Generic Salt Repository Science*, Los Alamos National Laboratory, USDOE Used Fuel Disposition Campaign, LA-UR-16-2732

Dakota, (2019), https://dakota.sandia.gov/, last accessed April 5, 2019.

dfnworks, (2019), https://dfnworks.lanl.gov/, last accessed April 5, 2019.

DOE (2011). *Used Fuel Disposition Campaign Disposal Research and Development Roadmap*. FCRDUSED-2011-000065 REV 0. Fuel Cycle Technologies, Office of Nuclear Energy, US Department of Energy, Washington, DC.

FEHM (2019), FEHM Website, https://fehm.lanl.gov/ accessed March 20th, 2019.

Harp, D.R., J.P., Ortiz, S. Pandey, S. Karra, D. Anderson, C.R. Bradley, H.S. Viswanathan, and P.H. Stauffer, (2018), *Pore-water storage enhancements and retardation of gas transport in fractured rock*, Transport in Porous Media, 124(2), September 2018.

Johnson, P. J., S. Otto, D. J. Weaver, B. Dozier, T. A. Miller, A. B. Jordan, N. G. Hayes-Rich, and P. H. Stauffer (2019), *Heat-Generating Nuclear Waste in Salt: Field Testing and Simulation*, Vadose Zone Journal, 18(1), doi: 10.2136/vzj2018.08.0160

Johnson, P. J., P. H. Stauffer, G. A. Zyvoloski, and S. M. Bourret (2018), *Experiments and Modeling to Support Field Test Design*, Los Alamos National Laboratory, Report: *LA-UR-18-28189*

Johnson, P.J., S.M. Bourret, H. Boukhalfa, F.A. Caprouscio, G.A. Zyvoloski, D.J. Weaver, S. Otto, M.M. Mills, E.M. Matteo, K.L. Kuhlman, J. Rutqvist, Y. Wu, and P.H. Stauffer, (2017a) *Test Plan Document for Thermal Testing in Salt*, M3SF-18LA010303013, LA-UR-1730762, 45p.

Johnson, P.J., H. Boukhalfa, D.J. Weaver, S. Otto, B.L. Dozier, P.H. Stauffer, (2017b) *Experiments and Modeling to Support Field Test Design*, M4SF-17LA010303022, LA-UR-17-27759, 98 p.

Jordan, A.B., H. Boukhalfa, F.A. Caporuscio; B.A. Robinson, P.H. Stauffer, (2015b), *Hydrous Mineral Dehydration around Heat-Generating Nuclear Waste in Bedded Salt Formations*, Environmental Science & Technology, 5:1-13. DOI: 10.1021/acs.est.5b01002.

Jordan, A.B., Boukhalfa, H., Caporuscio, F.A., Stauffer, P.H. *Brine Transport Experiments in Granular Salt* (2015b), Los Alamos National Laboratory, Report: LA-UR-15-26804.

Kuhlman, K. L., M. M. Mills, and E. N. Matteo (2017), *Consensus on Intermediate Scale Salt Field Test Design*, Sandia National Laboratory, Report: *SAND2017-3179R*

Kuhlman, K. L., M. M. Mills, C. G. Herrick, E. N. Matteo, P. Stuaffer, P. Johnson, H. Boukhalfa, D. Weaver, J. Rutqvist, and Y. Wu (2018), *Project Plan: Salt in Situ Heater Test*, Sandia National Laboratory, Report: *SAND-2018-4673R*

Kuhlman, K.L., Malama, B (2013), *Brine Flow in Heated Geologic Salt*, Sandia National Laboratory, Report: SAND2013-1944

LaGrit, (2019), lagrit.lanl.gov, last accessed April 5, 2019.

Lichtner, P.C., Hammond, G.E., Lu, C., Karra, S., Bisht, G., Andre, B., Mills, R., Kumar, J. (2015) *A massively parallel reactive flow and transport model for describing surface and subsurface processes*. PFLOTRAN user manual, http://www.pflotran.org/docs/user_manual.pdf.

Mariner, P.E., E.R. Stein, S.D. Sevougian, L.J. Cunningham, J.M. Frederick, G.E. Hammond, T.S. Lowry, S. Jordan, and E. Basurto, (2018). *Advances in Geologic Disposal Safety Assessment and an Unsaturated Alluvium Reference Case*, SFWD-SFWST-2018-000509, SAND2018-11858 R.

PFLOTRAN, (2019), https://www.pflotran.org/, last accessed April 5, 2019.

Robinson, B.A, N. Z. Elkins, J. T. Carter, (2012), *Development of a U.S. Nuclear Waste Repository Research Program in Salt, Nuclear technology* 180(1):122-138, DOI: 10.13182/NT12-A14524

Sevougian, S. D., E. R. Stein, M. B. Gross, G. E. Hammond, J. M. Frederick, P. E. Mariner, (2016), *Status of Progress Made Toward Safety Analysis and Technical Site Evaluations for DOE Managed HLW and SNF*, Sandia National Laboratory document, FCRD-UFD-2016-000082, Rev. 1, SAND2016-11232 R.

Stauffer, P.H., A. B. Jordan, D. J. Weaver, F. A. Caporuscio, J. A. Ten Cate, H. Boukhalfa, B A. Robinson, D. C. Sassani, K. L. Kuhlman, E. L. Hardin, S. D. Sevougian, R. J. MacKinnon, Y. Wu, T. A. Daley, B. M. Freifeld, P. J. Cook, J. Rutqvist, and J. T. Birkholzer, (2015). *Test proposal document for phased field thermal testing in salt*. Los Alamos National Laboratory, Report: FCRD-UFD-2015-000077

Vorocrust, (2019), https://ip.sandia.gov/technology.do/techID=208, last accessed April 5, 2019.

Zyvoloski, G.A., B. A. Robinson, Z. V. Dash, S. Kelkar, H. S. Viswanathan, R. J. Pawar, P. H. Stauffer, T. A. Miller, S. P. Chu (2012), *Software users manual* (UM) for the FEHM Application Version 3.1-3.X, Los Alamos National Laboratory, Report: LA-UR-12-2449